Simultaneous Second Harmonic Generation and Multiphoton Excited Photoluminescence in Anatase TiO2 Nano Powders

Christian Jonin, Estelle Salmon, Zacharie Behel, Faheem Ahmed, Mohammed Benali Kanoun, Chawki Awada, Pierre-François Brevet

Simultaneous Second Harmonic Generation and Multiphoton Excited Photoluminescence in Anatase TiO_2 Nano Powders

Christian Jonin[1*], Estelle Salmon[1], Zacharie Behel[1], Faheem Ahmed[2], Mohammed Benali Kanoun[2], Chawki Awada*[2], and Pierre –Francois Brevet[1]

[1] Institut Lumière Matière, Université de Lyon, UMR 5306 CNRS, Université Claude Bernard Lyon 1, 69622 cedex, Villeurbanne, France

[2] Department of Physics, College of Science, King Faisal University, P.O. Box 400, Al-Ahsa, 31982, Saudi Arabia

- Correspondence: christian.jonin@univ-lyon1.fr, cawada@kfu.edu.sa

Abstract:

Second Harmonic Generation (SHG) and Multiphoton Excited Photoluminescence (MEPL) are observed in retro-reflection mode from a 22 nm diameter anatase TiO_2 nanoparticle powder. Depth intensity profiles are obtained by scanning the fundamental beam focal point through the TiO_2 powder surface into its volume for the energy of the incident photons tuned around the anatase TiO_2 band-gap energy of 3.2 eV. Evidence for the appearance of both SHG and MEPL is presented, their relative contribution depending on the conditions of photo-excitation, in particular the fundamental wavelength and the focal point depth location. MEPL dominates at fundamental photon energies matching the band-gap energy whereas below and above the band-gap SHG is clearly seen. Depth intensity profiles exhibiting a rising edge determined by the fundamental laser beam focusing conditions and a decreasing edge determined by extinction and multiphoton scattering strongly differ between SHG and MEPL, SHG profiles being by far narrower than that of MEPL. Re-absorption of the emitted SHG and MEPL light occurs due to the spectral proximity with the TiO_2 band gap energy but excitation with fundamental light below band-gap further suggests that the intrinsic difference between the two SHG and MEPL processes is responsible for the contrasted depth profiles. This combined study where both SHG and MEPL occur presents perspectives in the study of the photonic properties of powder materials.

Keywords: TiO_2, Nanoparticles, Powder, Band-gap, Second Harmonic Generation, Multiphoton Excited Photoluminescence, Depth Profiles

1. Introduction

Second Harmonic Generation (SHG) is a nonlinear optical process whereby two photons at a fundamental frequency $\boldsymbol{\omega}$ are converted into a single photon at the harmonic frequency $\mathbf{2\omega}$. This process has been first observed in a quartz plate by Franken *et al.*[1] It has since been widely used in laser science to convert one frequency into its second harmonic. This phenomenon is forbidden in centrosymmetric media within the electric dipole approximation and has thus also been extended to the study of interfaces between two centrosymmetric media with great selectivity with respect to the bulk phase[2]. In the liquid phase, SHG is also possible due to instantaneous molecular orientational fluctuations and the method bears the name of Hyper Rayleigh Scattering (HRS)[3], namely the scattering of second harmonic light as a result of the absence of coherence between the emitting sources. It has been used to investigate the nonlinear optical properties of molecules and nanoparticles, plasmonic nanoparticles in particular, dispersed in a liquid solution.[4,5] Recent experiments have proposed new ways to study the effectiveness of SHG as well as its notable implication for pharmaceutical materials, in the context of powdered materials, effectively highly diffusing standard media[6]. Initially, SHG powder experiments were conducted by S.K. Kurtz and T.T. Perry[7] with the main objective to determine the absolute values of the second-order nonlinear susceptibility of materials. More recently, attention has been given to the SHG intensity arising from dielectric nano-and micro-powders and powder stacks[8,9].

Titanium dioxide (TiO_2) has been the subject of strong interest due to its photo-catalytic activity and therefore potential use in solar energy conversion, with a specific emphasis on the catalytic mechanisms following photo-excitation[10-13]. In this context, several methods have been used, and in particular optical SHG that has allowed to investigate the electronic states involved in the catalytic processes with the anatase and rutile forms of TiO_2 [14-17]. The anatase form has however a higher catalytic activity as compared to the other forms of TiO_2 like

rutile[18]. The objective of the present study performed on a 22 nm average diameter anatase TiO_2 nanoparticle powder is to investigate the simultaneous appearance of SHG and multiphoton excited photoluminescence (MEPL) as the fundamental wavelength is tuned through the band-gap energy. These two processes are of interest for further studies on the photo-catalytic mechanisms in this material because only MEPL may give rise to a catalytic activity due to the two-photon absorption step whereas SHG does not involve material photo-excitation[19]. Hence, SHG may be used as a reporter of the undergoing phenomena occurring during a photo-catalytic process. SHG and MEPL intensity profiles were thus recorded as the fundamental beam focal point is moved from air into the TiO_2 powder stack for different fundamental excitation wavelengths. This fundamental wavelength was tuned around the anatase TiO_2 band gap energy, the value of which is about 3.2 eV, corresponding to a wavelength of 390 nm. Hence, the exciting fundamental wavelength was tuned from 778 nm up to 822 nm yielding an SHG wavelength at half the fundamental wavelength ranging from 389 nm up to 411 nm. The MEPL emission wavelength is on the opposite determined by the material properties. This MEPL is either two or three photon excited depending on the fundamental wavelength.

2. Experimental Setup

The SHG experimental set-up described in Figure 1 has been depicted in detail elsewhere[20]. The nonlinear light source was a femtosecond Ti: sapphire laser (Coherent, model Mira 900) with a fundamental wavelength tuned from 778 up to 822 nm. The repetition rate was 80 MHz and the pulse duration was about 180 femtoseconds. A half-wave plate centered at 800 nm was placed along the beam to define the linear polarization angle of the fundamental input beam. A long-wavelength pass filter was placed to remove any second harmonic light generated prior to the sample. The two mirrors placed after this filter had a dielectric coating

to ensure that no second harmonic light was generated before the powder sample. This fundamental beam was focused onto the anatase TiO_2 powder by a X16 microscope objective with a numerical aperture of 0.32 providing a spot size of (5.0+/-0.5) microns in diameter. This microscope objective was placed on a vertical motorized translation stage (Thorlabs, model KMTS50E) to move the focal point from air to the air/powder interface and then into the bulk of the powder. The average power at the interface was about 500 mW. The SHG light and the MEPL generated from the sample were collected in retro-reflection. A dichroic mirror was placed above the objective to separate this light from the fundamental one. The harmonic beam was then focused by a 25 mm lens onto the entrance slit of the spectrometer (Spex, model 500 M) and then collected by a cooled CCD camera (Andor, model DU 440). The experiment was controlled with a custom-written LabVIEW software.

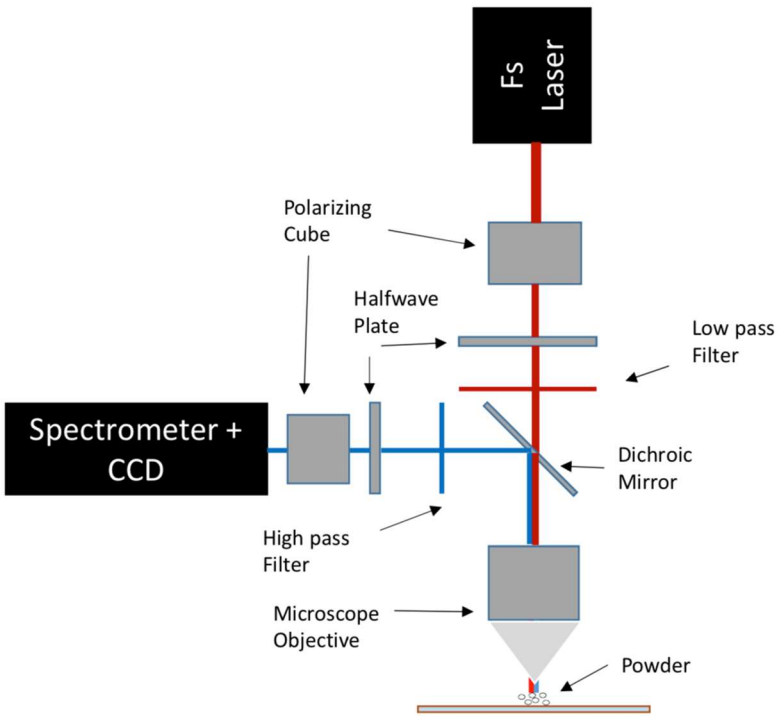

Figure 1: Schematics of the experimental setup.

3. Material and methods

The anatase TiO_2 nanoparticles were synthesized using the sol-gel method.[21] Briefly, 60 mL of titanium isopropoxide were mixed with 100 mL of ethanol. Then, titanium oxyde sols were formed by addition of 60 mL of deionized water. Stirring continued for 12h to form a gel. The final product with a white color was separated by centrifugation. The product was dried at 120°C and then calcinated at 450°C. The size of the TiO2 powder nanoparticles was about 22 nm in diameter, on average, see Figure 2 and Figure S1 along with X-ray diffraction (XRD) and Raman spectra provided in Figures S2 and S3 in Supplementary File as further characterizations. The powder was placed on a glass substrate and gently compressed with another glass plate removed afterwards in order to present a rather flat and as much as possible homogeneous surface.

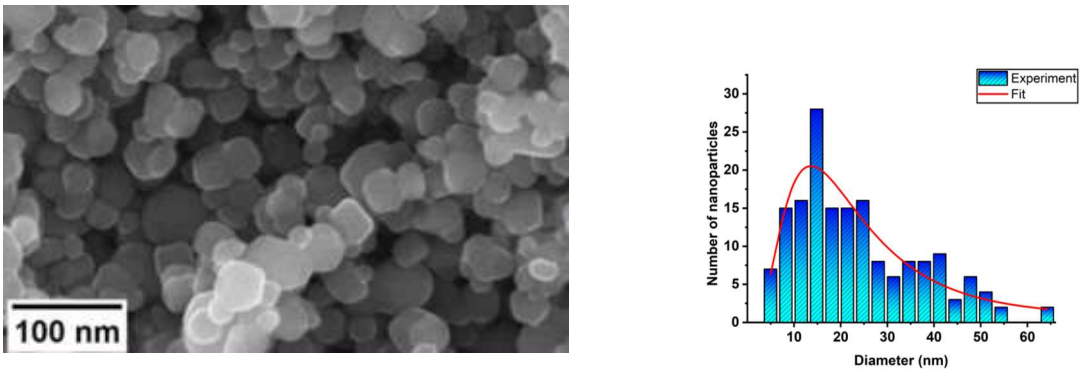

(a) (b)

Figure 2: (a) Field-Emission Scanning Electron Microscopy image of as-synthesized TiO2 nanoparticles, (b) Size distribution of the TiO2 nanoparticles with adjusted Log-Normal distribution.

Vertical profiles of the SHG and MEPL intensities were then obtained as follows: At each depth *z* position and fixed incident fundamental wavelength, the SHG and MEPL intensities were recorded where the horizontal axis provided the spectral decomposition, see Figure 3.

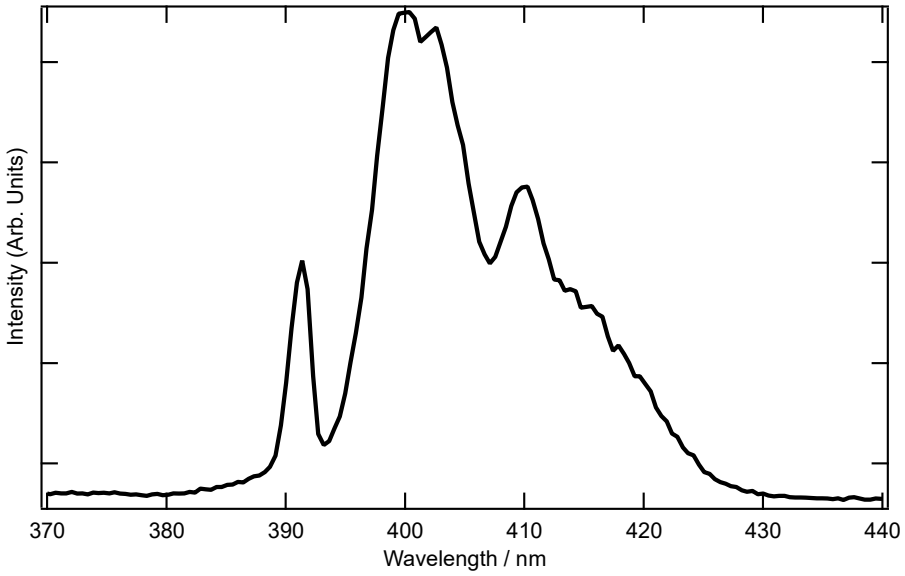

Figure 3: SHG and MPEL spectrum recorded at the depth position of the maximum SHG intensity. The incident fundamental wavelength is fixed at 782 nm.

As a result, with this procedure, a spectral analysis of the SHG and MEPL intensities was performed at each depth position of the beam focus, providing a combined SHG and MEPL spectrum at each depth position. In the spectral analysis, the SHG line was adjusted with a Gaussian function, the height of which providing the SHG intensity, possibly augmented with a broadband background, see Figure 3 where the broadband background is present under the SHG line at 391 nm. This procedure could only be performed when the SHG line was clearly visible, well separated from the broadband MEPL, the latter exhibiting several overlapping bands, see Figure 3 as well.

4. Results and Discussion

SHG and MEPL Spectra. On Figure 4 is depicted the spectral decomposition of the intensity collected in retro-reflection as the fundamental wavelength is tuned between 778 nm and 822 nm for a focal point located at or close to the air-powder interface. The latter interface is afterwards taken as the reference of the depth position, setting its position as z = 0. Three processes are clearly observed. The first one is SHG, the corresponding line at the harmonic wavelength following the simple law of the fundamental wavelength divided by two. The two other processes correspond to two- and three-photon excited photoluminescence. For two-photon excited photoluminescence, it is important to observe that the energy of the initial two photon absorption step is tuned from above to below the band-gap energy whereas for the three-photon excited photoluminescence, the corresponding energy of the three-photon absorption initial step is always above the band-gap energy. The SHG band is clearly observed as a Gaussian peak when it is located out of the MEPL intensity, at fundamental wavelengths in the range 778 - 790 nm and 800 - 820 nm but is barely visible in the range 790 – 800 nm when dwarfed by the MEPL intensity. Interestingly, this latter range corresponds to the band-gap wavelength since two-photon excitation MEPL (2P-MEPL) can occur. From this observation, it is concluded that the fundamental wavelength corresponding to the band gap is about 790 nm, corresponding to a harmonic wavelength of 395 nm instead of 389 nm, the harmonic wavelength corresponding to 3.2 eV.[21] In the short 778 - 790 nm wavelength range, 2P-MEPL is produced, although it is possible that higher multi-photon processes occur. In this range of wavelengths therefore, a study of the MEPL intensity dependence with the fundamental laser intensity would probably be inconclusive with a slope in the log-log plot between 2 and 3. However, in the long 800 - 820 nm wavelength range, the MEPL appears with an energy higher than that of the SHG intensity indicating that it must be three photon excited, i.e. 3P-MEPL. For the spectra close to 820 nm, this 3P-MEPL disappears because the laser intensity has dropped as a result of the end of the laser tuning range precluding any study

of the MEPL intensity dependence with the fundamental laser intensity. Also, in this spectral region where 3P-MEPL occurs above band gap, 3P-MEPL may also be re-absorbed, further decreasing its intensity see below. In the middle range 780 – 800 nm, MEPL appears simultaneously at shorter and longer wavelengths as compared to the SHG wavelength and therefore must arise from a combination of two- and three-photon excitation processes.

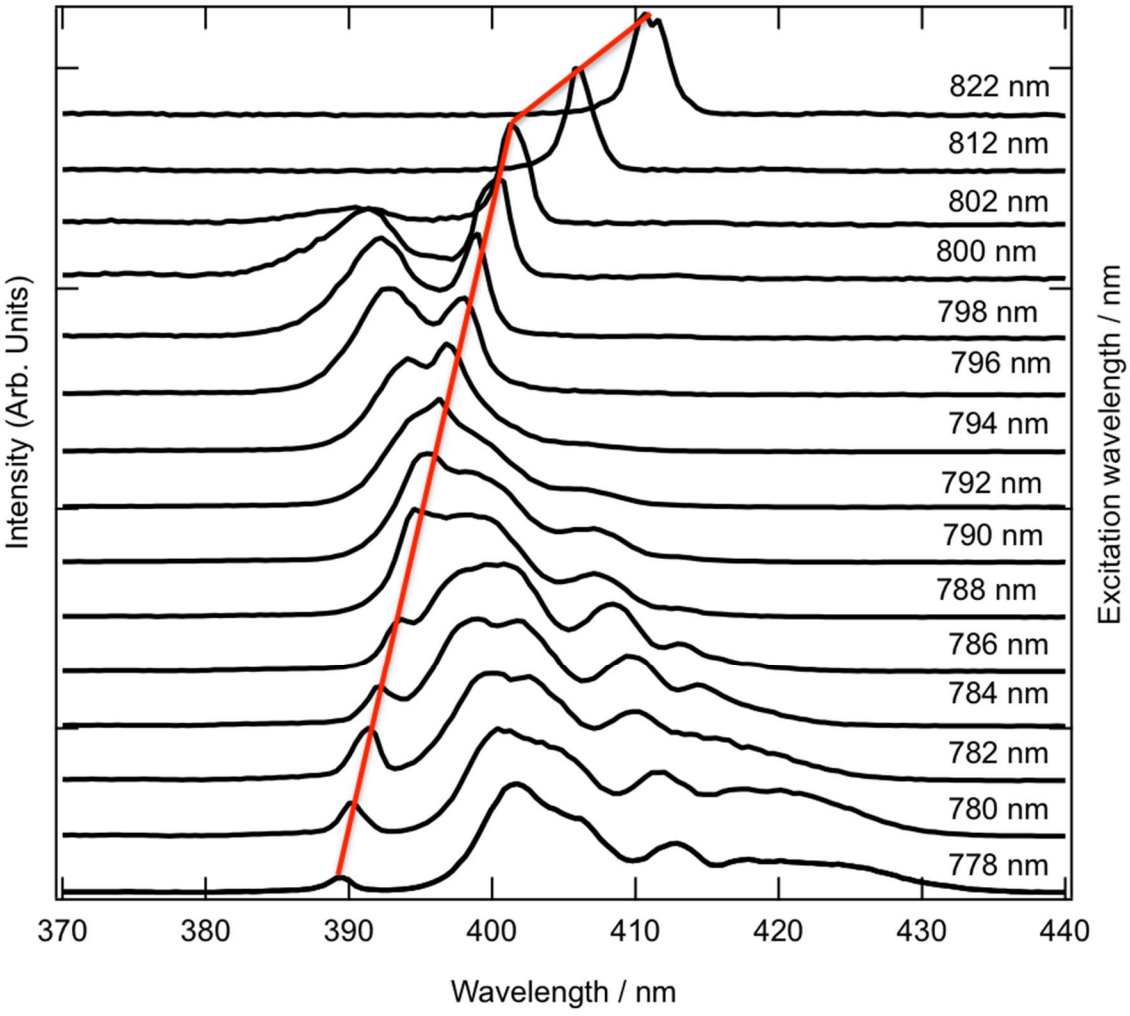

Figure 4: Spectra of the SHG and MEPL collected intensity as a function of the incident fundamental wavelength tuned between 778 nm and 822 nm for a laser focal point located at or close to the maximum of the intensity depth profiles. Red line is a guide to the eyes to follow the SHG line. Note that the last two spectra have an exciting wavelength shift of 10 nm instead of 2 nm for all the other spectra.

Considering the spectra reported in Figure 4 at different incident fundamental wavelength, it appears that the intensity depth profiles can be recorded separately for the SHG and the MEPL contributions with a careful choice of the spectral range of integration for the collected intensity. A 25 nm spectral width was taken for the SHG band whereas a 30 nm spectral width was chosen for the MEPL. However, in the middle range 780 – 800 nm around the fundamental wavelength of 792 nm, this separation is not possible and both SHG and MEPL are integrated together into the 30 nm spectral band.

Depth profiles. Intensity depth profiles were therefore obtained according to the method described above, as the focal point is translated from air, at negative depths, to the air-powder interface and into the bulk of the powder, on the positive depths side. The depth reference was set at the maximum of the SHG depth profiles. A depth step of 2 µm was used. Typical profiles are depicted in Figure 5.

All profiles exhibited an un-symmetric behavior, with a sharp rise on the negative depths side, i.e. on the air side of the air-powder interface, and a slower decrease on the positive depths, i.e. on the bulk powder side. This behavior is similar to that reported by Sanchez- Dena *et al* for the $LiNbO_3$ powders[20]. Depth profiles result from the combination of the squared longitudinal intensity profile of the translated focused fundamental TEM00 Gaussian beam on the rising edge and an exponential decay for the decreasing edge on the powder side at positive depths due to simultaneous extinction, due to multiple scattering and re-absorption when photon energies are above band gap. Both SHG and MEPL can be observed simultaneously when spectrally separated but may also overlap in some spectral regions. They nevertheless present rather different depth profile parameters. Assuming that the total

intensity $\boldsymbol{I_{Total}(z_0)}$ recorded at a given depth position $\boldsymbol{z_0}$ of the Gaussian beam focus results from their superposition, Eq.(1) can be written as follows using cylindrical symmetry and where integration over the transverse coordinates is implicit:

$$\boldsymbol{I_{Total}(z_0) = G_1 \int_0^{+\infty} \left| \frac{\exp(\beta_1 z)}{\sigma_1^2 + (z - z_{0,1})^2} \right|^2 dz + G_2 \int_0^{+\infty} \left| \frac{\exp(\beta_2 z)}{\sigma_2^2 + (z - z_{0,2})^2} \right|^2 dz} \quad (1)$$

where $\boldsymbol{G_1}$ and $\boldsymbol{G_2}$ are two general constants and $\boldsymbol{\beta_i = -3/l_i}$, *i = 1, 2*, $\boldsymbol{\sigma_i}$ is the width of the Lorentzian longitudinal Gaussian beam profile with maximum at $\boldsymbol{z_0}$ hence it corresponds to the beam Rayleigh parameter. Here, $\boldsymbol{l_1}$ and $\boldsymbol{l_2}$ are the characteristic lengths describing the loss of intensity in the powder at both fundamental and generated wavelength resulting from extinction, the photons having an energy above the TiO_2 band-gap, combined with multiple scattering in the powder. $\boldsymbol{l_1}$ corresponds to the characteristic length for SHG whereas $\boldsymbol{l_2}$ corresponds to that of MEPL.

Figure 5 gives depth profiles for three characteristic incident fundamental wavelengths belonging to the three different ranges observed above: short wavelength range at 778 nm, middle wavelength range at 792 nm closely matching the TiO2 band-gap energy and long wavelength range at 822 nm.

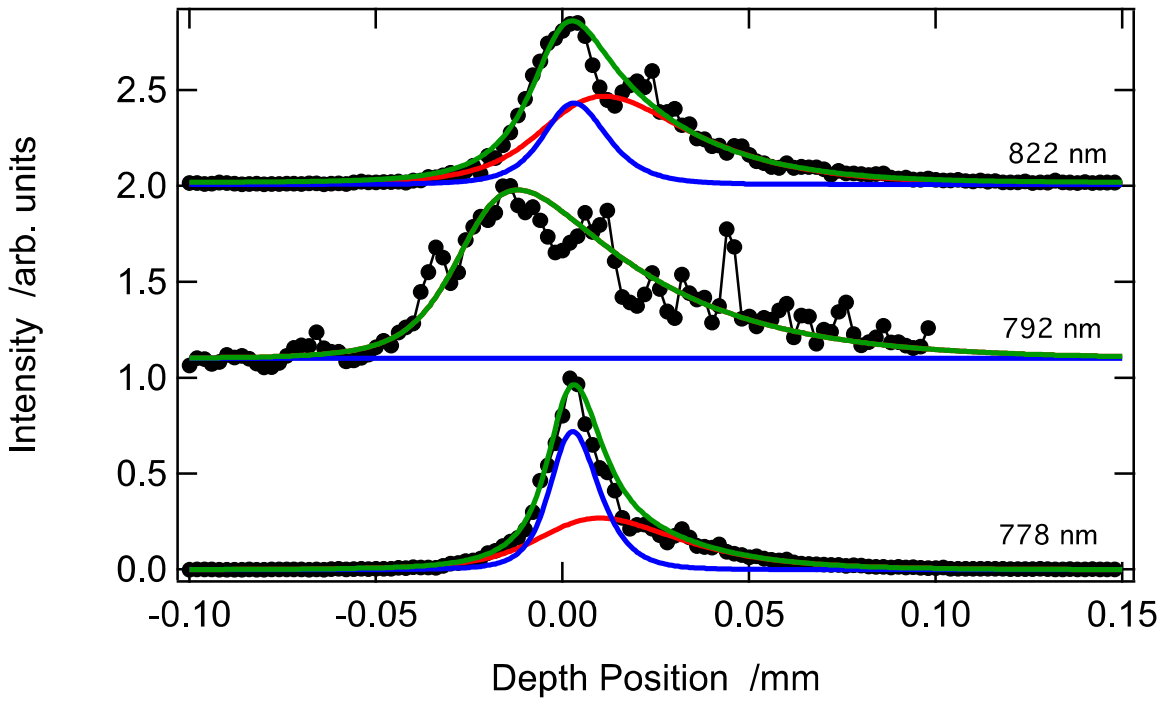

Figure 5: Intensity depth profiles recorded for three incident wavelengths for a 22 nm diameter TiO_2 nanoparticle powder as a function of the focal point depth position. (Black Disks) experimental points, (colored line) fits using Eq. (1), (blue) SHG only, (red) MEPL only, (green) SHG and MEPL combined. At 792 nm excitation, red and green profiles are superposed whereas the blue one is unnecessary and set to zero at all depths.

The depth profiles recorded for the fundamental wavelength of 778 and 822 nm are very similar with a rather sharp rise due to the beam focal point entering the powder and slower decrease due to the combination of extinction and multiple scattering. At a fundamental wavelength of 822 nm, 2P-MEPL is expected to be less prone to re-absorption because the photon energy is smaller than the band gap energy. Only 3P-MEPL is possibly re-absorbed. For these two depth profiles, the SHG line is clearly defined, well separated from the MEPL, as seen on the spectra reported in Figure 4. On the opposite, the depth profile recorded for a fundamental wavelength of 792 nm is totally dominated by the MEPL intensity contribution. SHG and MEPL cannot therefore be separated and the depth profile results from the total intensity collected. Using the model yielding Eq.(1), adjustment of the three intensity depth profiles of Figure 5 as a function of the focal point depth position was performed. Agreement

is satisfactorily obtained for the three profiles albeit with rather different parameters for SHG and MEPL, see Table 1.

As expected, at 778 nm and 822 nm fundamental wavelengths, the adjusted rising edge parameters are similar. For the rising edge, the characteristic length corresponds to the one expected for a X60 objective, in agreement with a previous work analysis[21]. However, at 792 nm fundamental wavelength, the intensity depth profile is dramatically different on both rising and decreasing edges as compared to the two previous profiles, likewise are the corresponding parameters. This is due to the dominant MEPL contribution, the properties of which are rather different from the SHG ones despite the same geometrical configuration. For the latter depth profile, the parameters correspond to that of MEPL only indicating that the SHG contribution is totally dwarfed by MEPL.

Table 1: Adjusted parameters for the intensity depth profiles as a function of the focal point position using Eq.(1).

Incident Wavelength (nm)	$\boldsymbol{\sigma_1}(\mu\boldsymbol{m})$	$\boldsymbol{l_1}(\mu\boldsymbol{m})$	$\boldsymbol{z_{0,1}}(\mu\boldsymbol{m})$	$\boldsymbol{\sigma_2}(\mu\boldsymbol{m})$	$\boldsymbol{l_2}(\mu\boldsymbol{m})$	$\boldsymbol{z_{0,2}}(\mu\boldsymbol{m}$	$\boldsymbol{G_1/G_2}$
778	10 +/- 1	12 +/- 1	0	25+/- 3	50 +/- 5	0	2.7 +/- 0.3
792	-----	-----	0	20 +/- 2	100 +/- 10	0	$+\infty$
822	10 +/- 1	15 +/- 2	0	25 +/- 3	60 +/- 6	0	1 +/- 0.1

All depth profiles are taken with the maximum of intensity defining the $\boldsymbol{z_{0,1} = 0}$ position. Adjustment of the MEPL profiles led to the same depth position reference. Within errors, SHG depth profiles on the one hand and MEPL depth profiles on the other hand exhibit the same parameters for the rising and falling edges, namely $\boldsymbol{\sigma_1}$ and $\boldsymbol{l_1}$ for the SHG profiles and $\boldsymbol{\sigma_2}$ and $\boldsymbol{l_2}$ for the MEPL profiles. These parameters are thus intrinsically attached to these two

processes. Also, SHG is always more prone to multiple scattering and re-absorption as compared to MEPL as seen by the much shorter $\boldsymbol{l_1}$ length as compared to $\boldsymbol{l_2}$. Likewise, a sharper rise is observed for SHG profiles as compared to MEPL as seen from the shorter Rayleigh parameter $\boldsymbol{\sigma_1}$ determined as compared to the MEPL one $\boldsymbol{\sigma_2}$. For the decreasing edge, this feature results from the wavelength of SHG which is always closer to the band-gap as opposed to MEPL, 2P-MEPL in this case, which is red-shifted and therefore below band-gap. 2P-MEPL is therefore less affected by re-absorption within the powder. Under this excitation condition where the two-photon excitation is below band gap, 2P-MEPL does not exist but three-photon excited 3P-MEPL takes over, see Figure 4 considering the spectra in the 798 - 802 nm range of incident wavelength. However, in this case it remains rather weak if not vanishing due to lower laser power. It is also re-absorbed because appearing above band-gap. Figure 6 depicts a 3P-MPEL depth profile.

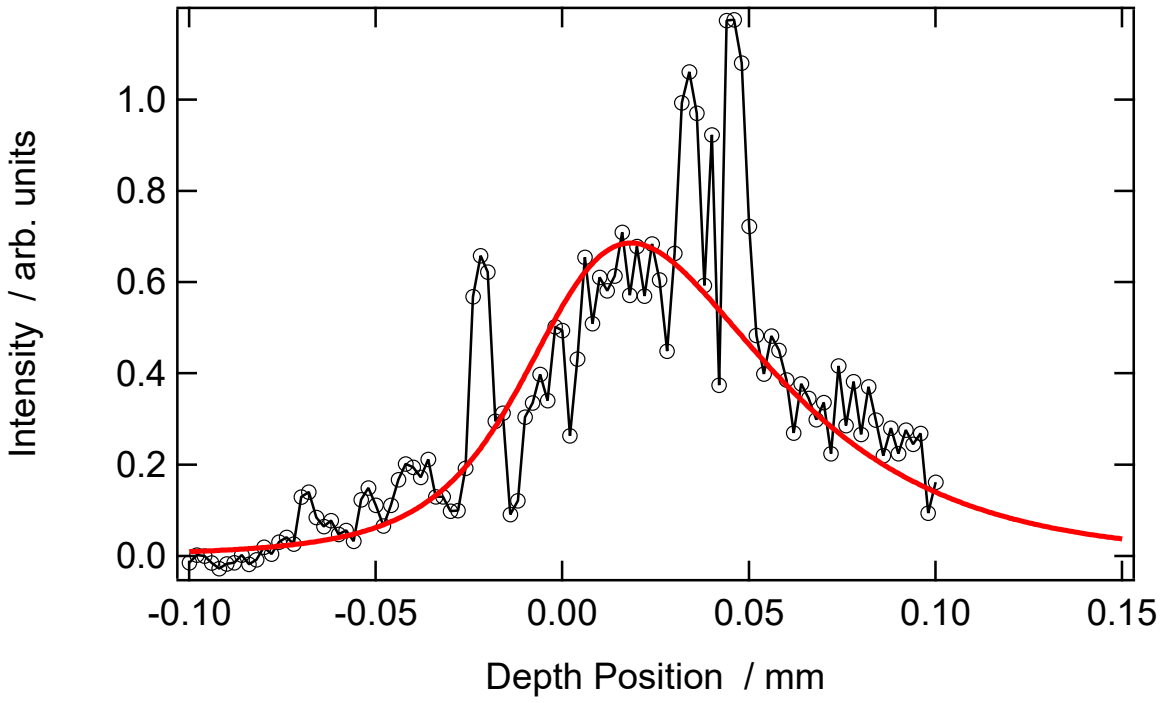

Figure 6: Intensity depth profile recorded for 800 nm incident wavelength for a 22 nm diameter TiO_2 nanoparticle powder as a function of the focal point position. (Disks) Experimental points, (redline) fit using Eq. (1). The disk points represent the 3P-MPEL profile corresponding to an integration width of 10 nm around 390 nm (maximum of the 3P-MEPL band).

This 3P-MPEL profile has been fitted using Eq.(1) with a single term, because the SHG contribution is not present, leading to the parameters as follows: $\boldsymbol{\sigma = 40}$ μm and $\boldsymbol{l = 100}$ μm, values comparable to those obtained for the 2P-MPEL profile. The expected sharper dependence with intensity due to the three photons required to perform the photo-excitation in the 3P-MEPL process does not appear clearly. Likewise, re-absorption follows the same process as in the case of 2P-MEPL and appears with a similar characteristic length.

In all the depth profiles recorded, small irregularities were noticed, see all profiles as well as Figures S4 in Supplementary File. These irregularities were not reproducible when the in-plane focus location was changed. Besides, the model cannot account for them, calling for further work to describe them.

Spectral dependence of depth profiles. To get a better view for comparison, Figure 7 provides 2D color plots of the spectral dependence of the depth profiles at the four incident wavelengths corresponding to Figure 4, evidencing the presence of both the SHG and MEPL bands with different properties. The SHG band moves according to the incident fundamental wavelength but blends with the 2P-MEPL band at 792 nm excitation. MEPL, red shifted from the SHG band, is also clearly seen as composed of several bands, as seen from its multiple peaks. The SHG band remains highly localized along the depth direction as opposed to MEPL, see Table 1.

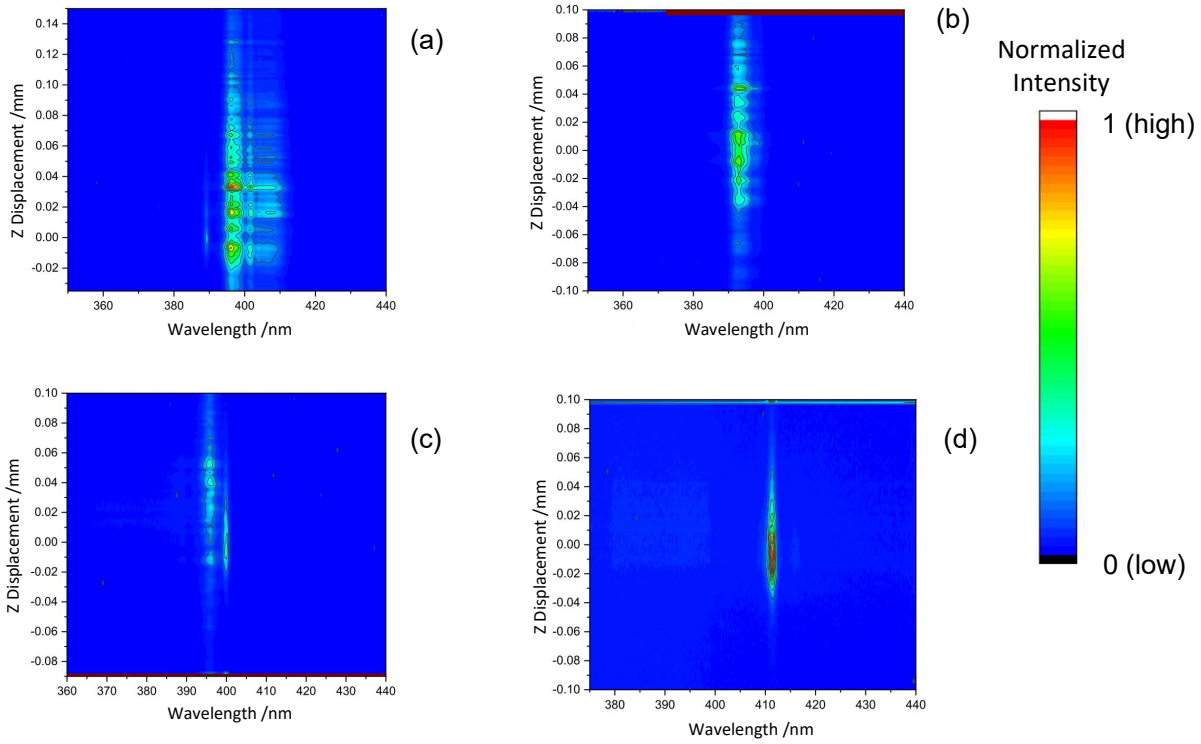

Figure 7: 2D color plots of the SHG and MEPL intensity as a function of depth and wavelength at (a) 778 nm, (b) 792 nm, (c) 800 nm and (d) 822 nm excitation fundamental wavelength. Horizontal axis is the collection wavelength and vertical axis is the focus depth position. Colour legend: from the lowest intensity (blue) to the highest intensity (red). All intensity graphs are normalized.

Figure 7(c) in particular provides the spectral analysis of the depth profile at 788 nm excitation of the 3P-MEPL appearing blue shifted from SHG. It appears very near the band-gap, slightly above, and is therefore considerably weaker than the two-photon excited one due to the extra photon required at excitation where the input laser power drops in this spectral tuning range and also due to re-absorption. Beyond 805 nm, it even disappears. It is interesting to note that for the 788 nm excitation, it remains with a much smoother decrease as compared to SHG with respect to depth position, the latter being less prone to re-absorption because it is red-shifted from the band gap. Further studies would require a power dependence to assess the exact number of photons involved in the excitation step.[22] It therefore raises the question of the fundamental differences between the two SHG and MEPL processes. Indeed, MEPL involves the generation of electron and holes that may propagate over some distances

before recombining, possibly longer than the TiO2 nanoparticles 22 nm average diameter. Hence, the MEPL process may stem from larger volumes as compared to SHG. SHG, on the opposite, does not involve charge generation and therefore is strictly restricted to the excitation volume. This is a clear example of the difference between the two processes. Besides, the band gap energy which is close to the collected photon energy provides further complexity due to the different processes possible, see Figure S5 in Supplementary Information file. Hence, with a single fundamental wavelength but two induced processes, different spatial volumes and depths are comparatively explored, resulting in fine insights into the light interaction with the nanoparticle powder.

5. Conclusions

We have reported intensity depth profiles for both SHG and MEPL from a 22 nm diameter nanoparticle TiO_2 powder for the fundamental wavelength tuned over the band gap. The profiles are spectrally analyzed in order to yield a careful comparison between the two SHG and MEPL processes. MEPL can be two- and three-photon excited depending on the energy of the fundamental incident beam with respect to the band-gap energy. A simple model involving a Gaussian beam and combination of extinction and multiple scattering is then used to quantitatively adjust the intensity depth profiles as a function of the focal point depth position and perform a quantitative comparison. Small irregularities noticed were not accounted for by this model and remain to be studied in greater detail. MEPL is shown to exhibit weaker geometrical constraints and therefore much smoother profiles as compared to SHG that presents both sharp rising and falling edges. This difference is principally attributed to re-absorption. Nevertheless, the exact nature of the two SHG and MEPL processes is clearly revealed in these contrasted depth profiles. These results suggest that combination of

SHG and MEPL present an interesting perspective to study light activated processes into TiO2 powders studies since MEPL should participate to this process due to the generation of charges whereas SHG does not.

6. Acknowledgments:

The authors extend their appreciation to the Deputyship for Research & Innovation, Ministry of Education in Saudi Arabia for funding this research work through the project number 1063.

7. References

(1) P.A. Franken, A.E. Hill, C.W. Peters, G. Weinreich, Generation of Optical Harmonics, Phys. Rev. Lett., 1961, 7, 118.

(2) F. Brown, R. E. Parks, A. M. Sleeper, Nonlinear Optical Reflection from a Metallic Boundary, Phys. Rev. Lett., 1965, 14, 1029.

(3) R.W. Terhune, P.D. Maker, C.M. Savage, Measurements of Nonlinear Light Scattering, Phys. Rev. Lett., 1965, 14, 681.

(4) K. Clays, A. Persoons, Hyper Rayleigh Scattering in Solution, Phys. Rev. Lett., 1991, 66, 2980.

(5) J. Nappa, G. Revillod, I. Russier-Antoine, E. Benichou, C. Jonin, P. F. Brevet, Electric dipole origin of the second harmonic generation of small metallic particles, Phys. Rev. B, 2005, 71, 165407.

(6) A.U. Chowdhury, S. Zhang, G.J. Simpson, Powders analysis by second harmonic generation microscopy, Anal. Chem., 2016, 88, 3853.

(7) S.K. Kurtz, T.T. Perry, A powder technique for the evaluation of nonlinear optical materials, J. Appl. Phys., 1968**,** 39, 3798.

(8) O. Sanchez-Dena, E.V. García-Ramírez, C.D. Fierro-Ruíz, E. Vigueras-Santiago, R. Farías, J.A. Reyes-Esqueda, Effect of size and composition on the second harmonic generation from lithium niobate powders at different excitation wavelengths, Mater. Res. Express, 2017, 4, 035022.

(9) U.S. Kestur, D. Wanapun, S.J. Toth, L.A. Wegiel, G.J. Simpson, L.S. Taylor, Nonlinear Optical Imaging for Sensitive Detection of Crystals in Bulk Amorphous Powders, J. Pharma. Sci., 2012, 101, 4201.

(10) A. Fujishima, K. Honda, Electrochemical Evidence for the Mechanism of the Primary Stage of Photosynthesis, Bull. Chem. Soc. Japan, 1971, 44, 1148.

(11) L. Lin, Z. Jiang, C. Zhu, X. Hu, X. Zhang, H. Zhu, J. Fan, Enhanced optical absorption and photocatalytic activity of anatase TiO_2 through (Si,Ni) codoping, J. Appl. Phys. Lett., 2012, 101, 062106.

(12) W.J. Yin, H. Tang, S.H. Wei, M.M. Al-Jassim, J. Turner, Y. Yan, Band structure engineering of semiconductors for enhanced photoelectrochemical water splitting: The case of TiO_2, Phys. Rev. B*,* 2010, 82, 045106.

(13) L. Liu, Y. Jiang, H. Zhao, J. Chen, J. Cheng, K. Yang, Y. Li, Engineering Coexposed (001) and (101) Facets in Oxygen-Deficient TiO_2 Nanocrystals for Enhanced CO_2 Photoreduction under Visible Light. ACS Catal*.,* 2016, 6, 1097.

(14) K. Fukui, H. Onishi, Y. Iwasawa, Atom-Resolved Image of the TiO2(110) Surface by Noncontact Atomic Force Microscopy, Phys. Rev. Lett., 1997, 79, 4202

(15) A.N. Shultz, W. Jang, W.M. Hetherington III, D.R. Baer,L-Q. Wang, M.H. Engelhard, The adsorption of liquid and vapor water on TiO_2(110) surfaces: the role of defects, Surf. Sci., 1995, 339, 114.

(16) E. Kobayashi, G. Mizutani, S. Ushioda, Surface Optical Second Harmonic Generation from Rutile TiO2(110) in Air, Japan J. Appl.Phys., 1997, 36, 7250.

(17) E. Kobayashi, T. Wakasugi, G. Mizutani, S. Ushioda, Optical Second Harmonic Generation from Periodic Steps on Rutile TiO_2(110), Surf.Sci., 1998, 402, 537.

(18) H. Tang, F. Levy, H. Berger, P. E. Schmid, Urbach tail of anatase TiO_2, Phys. Rev. B, 1995, 52, 7771

(19) R.W. Boyd, Nonlinear Optics, Academic Press, New York, 2008.

(20) O. Sanchez-Dena, Z. Behel, E. Salmon, E. Benichou, J.A. Reyes-Esqueda, P.F. Brevet, Ch. Jonin, Polarization-resolved second harmonic generation from LiNbO3 powders, Opt. Mat., 2020, 107, 110169.

(21) A. Faheem, M. B. Kanoun, C. Awada, Ch. Jonin, P-F Brevet, An Experimental and Theoretical Study on the Effect of Silver Nanoparticles Concentration on the Structural, Morphological, Optical and Electronic Properties of TiO2 Nanocrystals, Crystals, 2021, 11, 1488.

(22) D.J. Morrow, M.P. Hautzinger, D.P. Lafayette II, J.M. Scheeler, L. Dang, M. Leng, D.D. Kohler, A.M. Wheaton, Y. Fu, I.A. Guzei, J. Tang, S. Jin, J.C. Wright, Disentangling Second Harmonic Generation from Multiphoton Photoluminescence in Halide Perovskites using Multidimensional Harmonic Generation, J. Phys. Chem. Lett., 2020, 11, 6551.

Supplement Information file

Simultaneous Second Harmonic Generation and Multiphoton Excited Photoluminescence in Anatase TiO_2 Nano Powders

Christian Jonin[1*], Estelle Salmon[1], Zacharie Behel[1], Faheem Ahmed[2], Mohammed Benali Kanoun[2], Chawki Awada*[2], and Pierre –Francois Brevet[1]

1. Characterization of the anatase TiO_2 powder

SEM pictures of the TiO2 nanoparticle powder sample to provide further characterization..

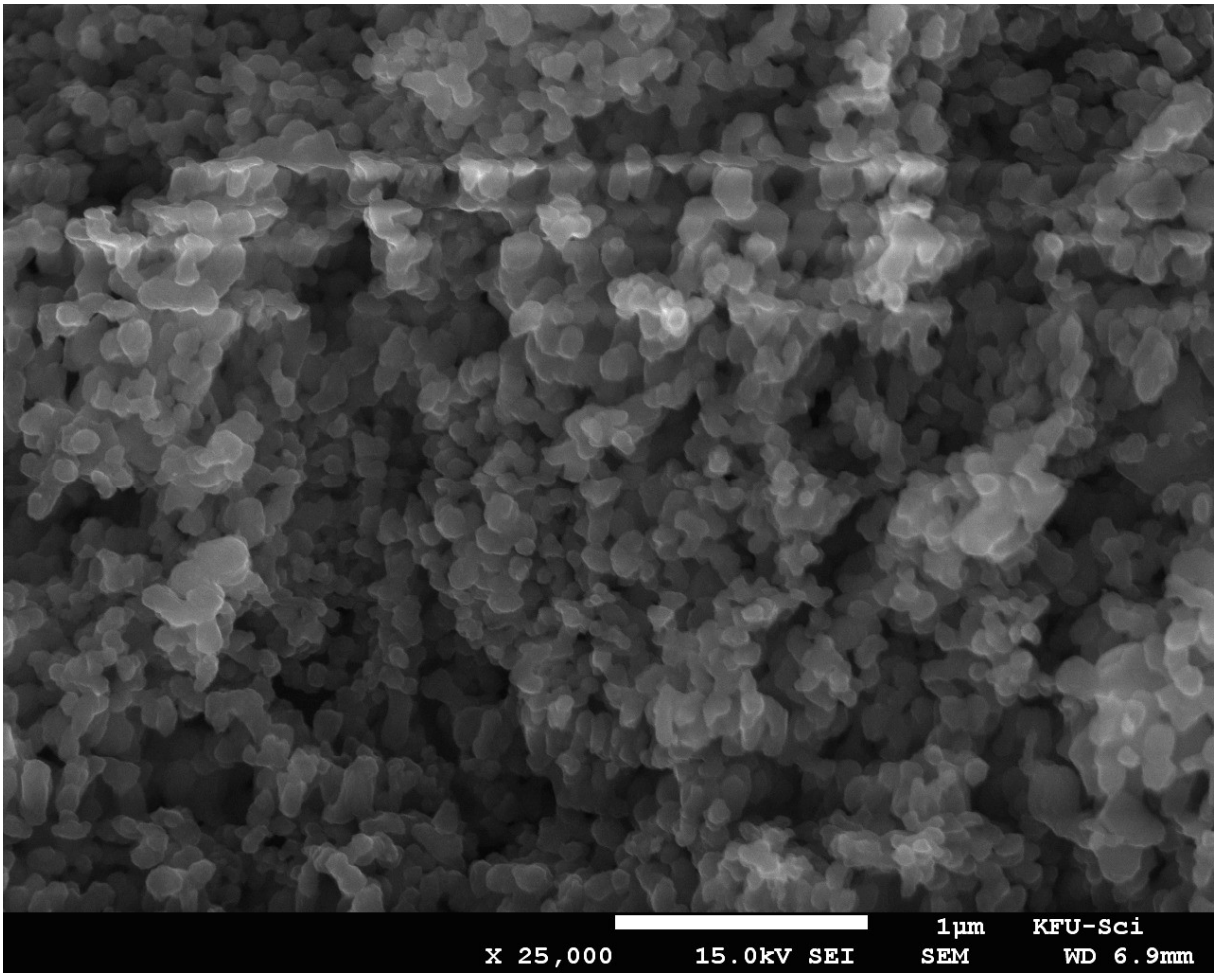

Figure S1 : Scanning Electron Micrograph (SEM) image of the anatase TiO_2 powder sample

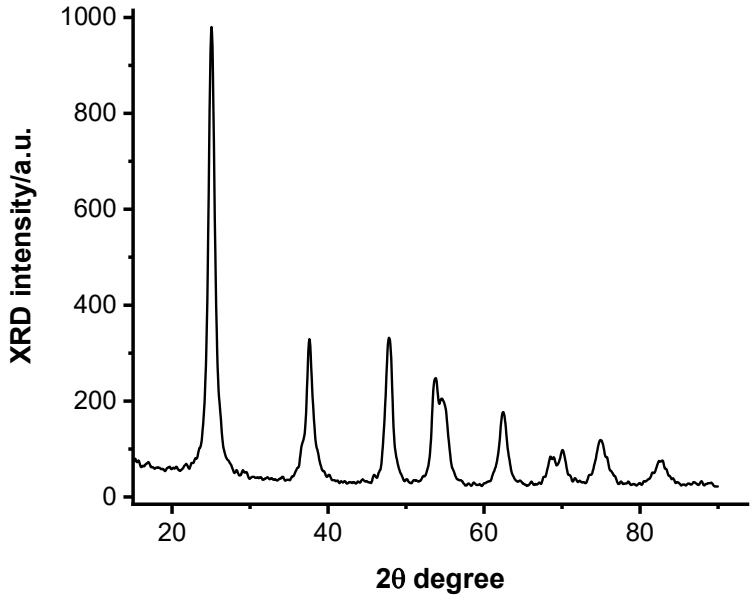

Figure S2 : X-ray Diffraction (XRD) patterns of TiO_2 nanoparticles. The XRD patterns confirm an anatase phase of the synthetized sample (JCPDS card no. 21-1272)

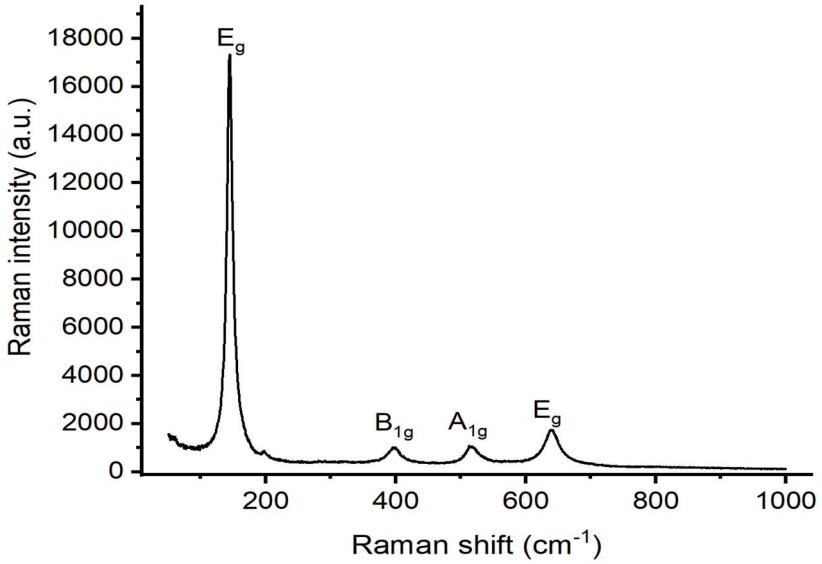

Figure S3 : Raman spectra of pure TiO_2 nanoparticles. An intense Raman peak at 145 cm^{-1} is observed, which can be assigned to the Eg optical Raman mode of anatase TiO_2. The other Raman peaks at 196 cm^{-1},394 cm^{-1}, 512 cm^{-1}, and 636 cm^{-1} were assigned to E_g, B_{1g}, A_{1g}, and E_g Raman modes of anatase TiO_2, respectively.

2. Intensity depth profiles at different location at the air-powder surface.

Two different profiles recorded at the 778 nm excitation avelength for the SHG intensity collected at two different location within the (X, Y)-plane of the air-powder interface providing a view on the in-plane reproducibility.

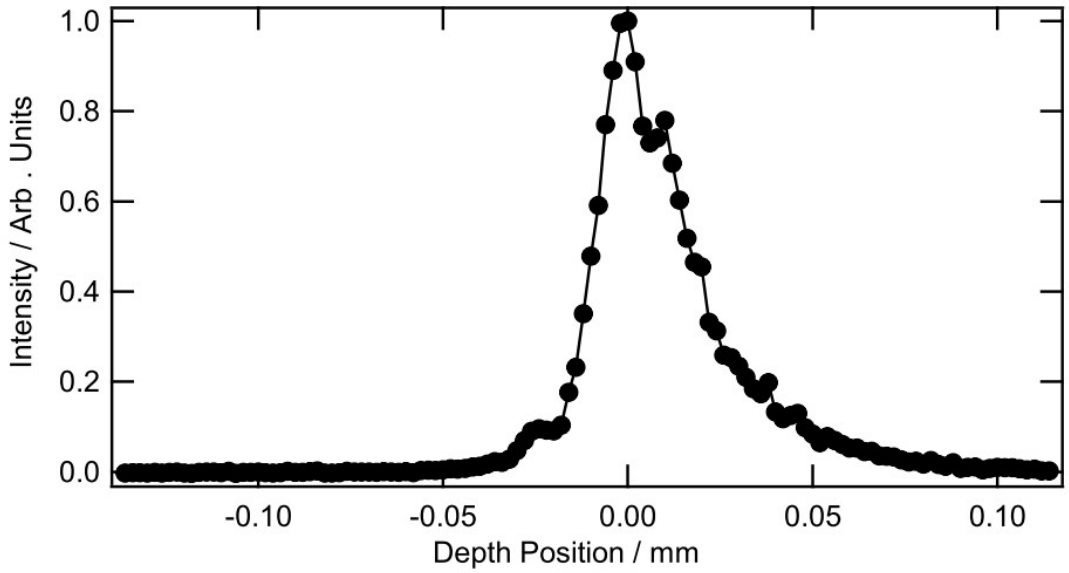

(a)

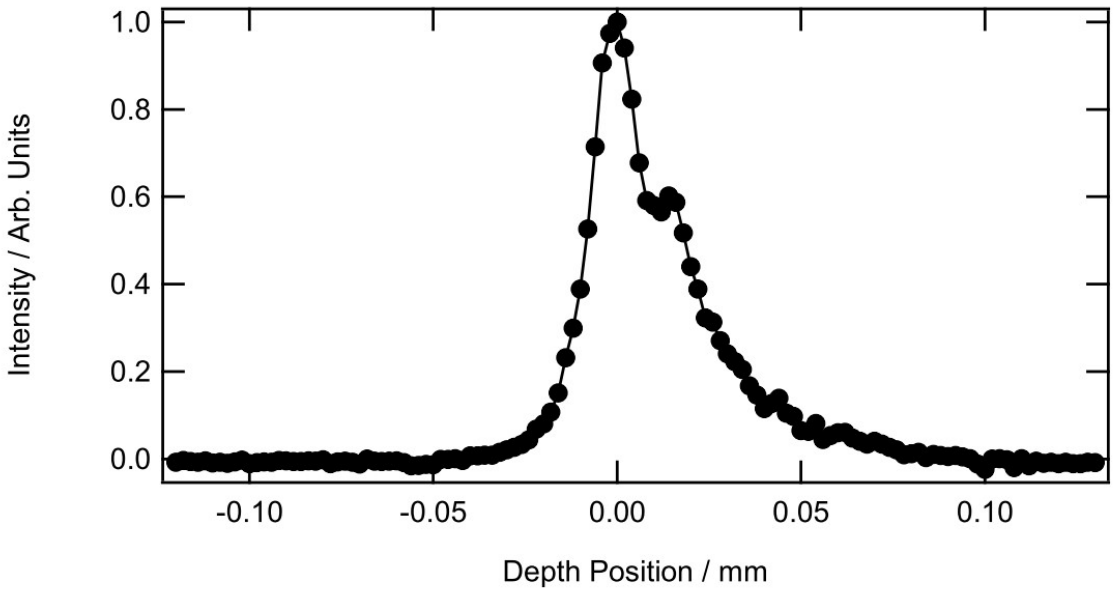

(b)

Figure S4 (a) – (b) : Intensity depth profiles recorded for 778 nm incident wavelength for a 22 nm diametre TiO2 nanoparticle powder at two different positions of the fundamental beam at the air-powder interface. (Black Disks) experimental points.

3. Schematic of the three different processes observed

Schematics of the different processes involved during these experiments, showing the SHG and 2P- / 3P-MEPL processes.

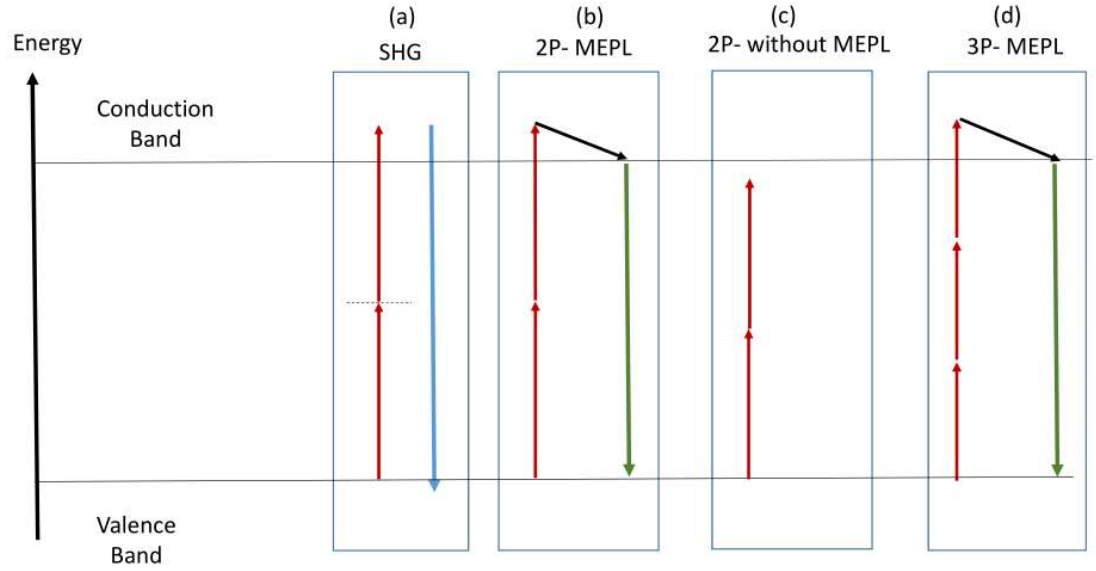

Figure S5 : Energy diagram distinguishing the four different nonlinear processes occurring during irradiation of the 22 nm diameter TiO2 powder, namely (a)SHG, 2P-MEPL (b), 2P without absorption (c) and 3P-MEPL(d).